

Spectral Inversion of Multi-Line Full-Disk Observations of Quiet Sun Magnetic Fields

H. Balthasar · M.L. Demidov

Received: / Accepted: / Published online:

Version: August 29, 2018
© Springer Science+Business Media B.V. 2011

Abstract Spectral inversion codes are powerful tools to analyze spectropolarimetric observations, and they provide important diagnostics of solar magnetic fields. Inversion codes differ by numerical procedures, approximations of the atmospheric model, and description of radiative transfer. *Stokes Inversion based on Response functions* (SIR) is an implementation widely used by the solar physics community. It allows to work with different atmospheric components, where gradients of different physical parameters are possible, *e.g.*, magnetic field strength and velocities. The spectropolarimetric full-disk observations were carried out with the Stokesmeter of the *Solar Telescope for Operative Predictions* (STOP) at the Sayan Observatory on 3 February 2009, when neither an active region nor any other extended flux concentration was present on the Sun. In this study of quiet Sun magnetic fields, we apply the SIR code simultaneously to 15 spectral lines. A tendency is found that weaker magnetic field strengths occur closer to the limb. We explain this finding by the fact that close to the limb, we are more sensitive to higher altitudes in an expanding flux tube, where the field strength should be smaller since the magnetic flux is conserved with height. Typically, the inversions deliver two populations of magnetic elements: (1) high magnetic field strengths (1500–2000 G) and high temperatures (5500–6500 K) and (2) weak magnetic fields (50–150 G) and low temperatures (5000–5300 K).

Keywords: Magnetic fields – Photosphere · Spectral Line – Intensity and Diagnostics · Polarization – Optical · Center-Limb Observations

1. Introduction

The small-scale organization of solar magnetic fields still holds many mysteries. Even with observations from space, where the Japanese *Hinode* mission (Suematsu *et al.*,

H. Balthasar (✉)
Leibniz-Institut für Astrophysik Potsdam (AIP),
An der Sternwarte 16, 14482 Potsdam, Germany
email: hbalthasar@aip.de

M.L. Demidov
Institute of Solar-Terrestrial Physics, Siberian Branch,
Russian Academy of Sciences, 664033 Irkutsk, P.O. Box 291, Russia
email: demid@iszf.irk.ru

2008) now routinely provides spectropolarimetric data in the two Fe I $\lambda 630.15$ nm and $\lambda 630.25$ nm lines with high angular resolution and high polarimetric precision, the fundamental spatial scales remain just beyond our grasp. Various investigations based on *Hinode* data, however, demonstrate the rapid advances in understanding solar small-scale magnetic fields (Ishikawa and Tsuneta, 2011; Kontogiannis, Tsiropoula and Tziotziou, 2011; Manzo Sainz, Martínez González and Asensio Ramos, 2011; Thornton and Parnell, 2011). The next generation of ground-based telescopes with apertures larger than 1-meter diameter and future space missions such as the *Solar Orbiter* will certainly provide magnetic field data with even higher angular resolution. But there are some indications that the smallest building blocks of solar magnetic fields might be as small as 10 km (Stenflo, 2010, 2011). This would be a challenge even for the largest telescopes, which are currently on the drawing boards.

The *Helioseismic and Magnetic Imager* (HMI) on board of the *Solar Dynamics Observatory* (SDO, Norton *et al.*, 2006; Borrero *et al.*, 2011) opens other avenues to understanding solar magnetism. Full-Stokes observations are carried out with moderate spectral resolution in the Fe I $\lambda 617.33$ nm line with a high cadence of 45 s covering the entire solar disk with a spatial resolution of about one second of arc. Besides exploiting these data in the context of helioseismology, they allow us to study the dynamics as well as the long-term evolution of solar magnetic fields. Finally, 3-D magneto-hydrodynamic (MHD) simulations (*e.g.*, Danilovic, Schüssler and Solanki, 2010) provide another perspective elucidating the nature of solar small-scale magnetic fields.

In this study, we use a complementary approach to extract the inner (hidden) properties of magnetic fields contained inside the resolution element of the Stokesmeter of the *Solar Telescope for Operative Predictions* (STOP) at the *Sayan Solar Observatory* near Irkutsk, Russia. In a two-components approach, where the magnetic and non-magnetic components have different filling factors within the resolution elements, as many spectral lines as possible are necessary for reliable magnetic field diagnostics (Demidov and Balthasar, 2012). We studied the center-to-limb variation (CLV) of quiet Sun magnetic fields, *i.e.*, the dependence of physical parameters on the cosine of the heliocentric angle $\mu = \cos(\vartheta)$, using the code *Stokes Inversion based on Response functions* (SIR) (Ruiz Cobo and del Toro Iniesta, 1992), where multi-line diagnostics and the two-components approach can be implemented in a straightforward manner. The present investigation combines three important aspects: (1) we explore the Stokesmeter observations (Stokes I and V/I_c profiles) in 15 spectral lines simultaneously, (2) we analyze observations covering practically the whole range of heliocentric angles ϑ , and (3) we analyze signals of extremely small degrees of polarization. Our investigation complements high-resolution observations and potentially links them to spatially unresolved stellar observations.

2. Observations

This study is an extension of our previous investigations (Demidov and Balthasar, 2009, 2012), where we analyzed Stokesmeter data of 15 spectral lines, which were obtained with the STOP telescope (Demidov *et al.*, 2002) in February 2009. A detailed description of the instrument, the observing procedure, and examples of Stokes profiles, as

well as the line parameters can be found in these publications. Nominally, spectra are obtained for areas covering $100''$ on a raster with an equidistant grid spacing of $91''$ covering the entire solar disk. In this study, this spacing was kept but the areas were reduced to $10'' \times 10''$. Spectra for 325 of such equidistantly spaced pixels were recorded with an integration time of 8 s. Thus, a raster scan of the entire solar disk takes about 70 min including the time to position the telescope and the polarimeter. The noise level in the continuum is used to estimate the polarimetric accuracy. We find an *rms*-value of 0.5×10^{-4} .

Solar activity was extremely low during the observations in February 2009. No sunspot was present during the first half of the month and only a small emerging flux region received an NOAA number on 11 February 2009. The appearance of the quiet Sun magnetic fields resembles that of a salt-and-pepper pattern, which covered the entire solar surface. We selected 3 February 2009 for this study because on this day, the seeing conditions were good and a large number of pixels exceeded the noise threshold of the Stokes V/I_c signal. To validate our observations, we averaged a magnetogram of the *Michelson Doppler Imager* (MDI) on board the *SOlar and Heliospheric Observatory* (SOHO) using the same grid and size of pixels as in the STOP Stokesmeter observations. The used magnetogram was obtained on the same day, but some hours later. The visual appearance of the two magnetic field rasters is surprisingly similar.

In this study, we distinguish strictly between the magnetic flux density as we derive it from our classical method (Demidov *et al.*, 2008) and the magnetic field strength B we obtain for the magnetic component from the SIR-inversions. In contrast to our previous studies, we use now the symbol Φ for the magnetic flux density. Magnetic features in the quiet Sun are small and do not fill our resolution element, thus we deal with flux densities. From the inversion, we derive also a filling factor and therefore we consider the inversion result as magnetic field strength. The magnetic flux densities $\Phi_{523.3}$ and $\Phi_{525.0}$ are shown in Figure 1 for the pair of Fe I $\lambda 523.3$ nm and $\lambda 525.0$ nm lines. There are two pixels on both maps with remarkably high flux densities – one near the eastern limb at $\mu = 0.65$, and another close to disk center at $\mu = 0.98$. Just comparing the flux densities of these central and limb pixels in the two Fe I lines provides a first hint for a strong CLV of the magnetic flux density ratio \bar{R} . The flux densities are $\Phi_{523.3} = 41.0$ G and $\Phi_{525.0} = 15.5$ G for the central and $\Phi_{523.3} = 31.8$ G and $\Phi_{525.0} = 20.6$ G for the limb pixels, respectively. This is in good agreement with the strong CLV of the magnetic flux density ratio $R(\mu) = \Phi_{523.3}(\mu)/\Phi_{525.0}(\mu) = 1.74 - 2.43\mu + 3.43\mu^2$ with a disk-averaged ratio of $\bar{R} = 1.97 \pm 0.02$, which was measured by Demidov and Balthasar (2009).

We introduce now the parameter A which is the integrated absolute value of Stokes V/I_c divided by 15 (the number of lines), shown in Figure 1. This parameter was used as a measure of the polarization signal because the measured flux densities in different lines vary from pixel to pixel. The majority of pixels has polarization signals, which are too weak to yield reliable inversion results. Pixels with A below 0.025 were removed from further analysis. According to visual inspection, polarization signals are above the noise level if A exceeds this threshold. This threshold corresponds to a magnetic flux density of roughly 3.5 G from the Fe I $\lambda 525.0$ nm line. In addition, we did not consider pixels closer to the limb than $\mu = 0.6$. A total of 37 pixels surpassed these criteria and form the basis for subsequent analysis.

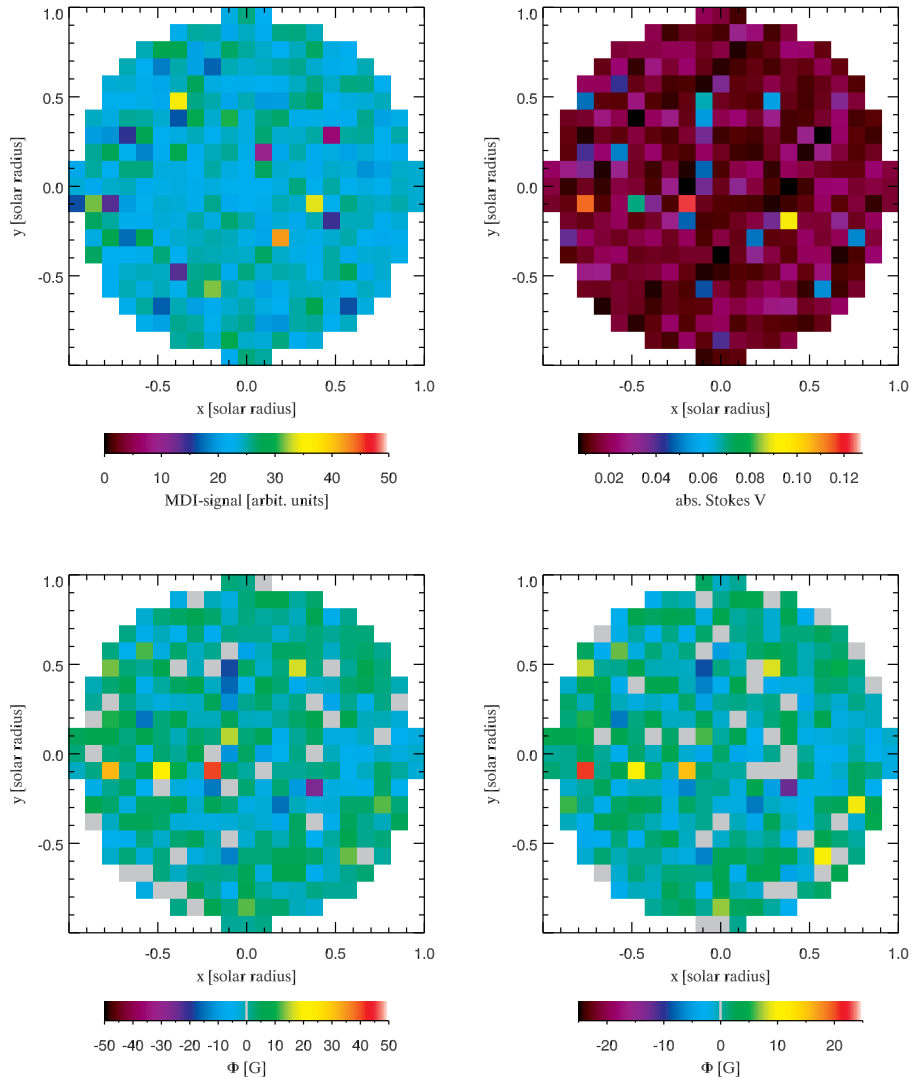


Figure 1. Averaged MDI-magnetogram (upper left) and integrated absolute values of the Stokes V/I_c parameter A (upper right). The bottom row shows full-disk magnetograms observed simultaneously in the Fe I $\lambda 523.3$ nm (left) and $\lambda 525.0$ nm (right) lines on 3 February 2009. Each pixel corresponds to $10'' \times 10''$. Note that the size of the pixels is not to scale.

In a first step, SIR was applied to these pixels. The starting model was basically the same as in Demidov and Balthasar (2012). A pixel was considered to be composed of non-magnetic (*Harvard Smithsonian Reference Atmosphere*, HSRA, Gingerich *et al.*, 1971) and magnetic components with a height-independent filling factor f as a free parameter. The magnetic component has the temperature stratification $T(\tau)$ of the model of Solanki and Brigljevič (1992), but a different stratification for the magnetic field.

From this initial guess, temperatures were calculated with five nodes in optical depth τ . In contrast to Demidov and Balthasar (2012), the magnetic field strength B was considered to be constant with depth and oriented vertically with respect to the solar surface. The angle γ between the line-of-sight (LOS) and the direction of the field lines coincides either with ϑ or with $180^\circ - \vartheta$ depending on the sign of Stokes V/I_c . Intensity spectra are normalized for the inversions in a way that they follow the CLV of Equation 10 in the article of Pierce and Slaughter (1977), since we do not know the exact variation of the atmospheric transparency during our observations.

3. Results

As an example, a comparison of observed and inverted spectral line profiles is shown in Figure 2, which also depicts the parameters of the starting model and the inversion results. The magnetic filling factor in this special case is 0.016 ± 0.006 . The inverted profiles for the magnetic and non-magnetic components agree very well with the observations. In quiet Sun regions, we assumed that hot rising granules contribute more in deep atmospheric layers. Therefore, only a shift of the entire Doppler velocity curve was allowed in the inversions. The displayed error ranges are delivered by the SIR code. Temperatures become rather unreliable in very high layers, and the steep temperature increase of the magnetic component above $\log \tau_{500} = -3.5$ is most likely not realistic.

The SIR code was applied to all pixels with Stokes V/I_c signals above the noise threshold defined in Section 2. The inverted magnetic field strengths B and filling factors f for these pixels are presented in the upper left and right panels of Figure 3, respectively. The inversions yield two populations with a distinct dependence on the heliographic angle ϑ : (1) pixels with kilo-Gauss strengths (larger than 1200 G) and very small filling factors (0.005 – 0.041) in the central part of the solar disk and (2) pixels with rather weak field strengths (less than 200 G) and large filling factors (up to 0.5) closer to the solar limb. All strong field cases occur at $\mu > 0.85$ and all weak field cases at $\mu < 0.95$.

Knowing the inverted magnetic field strengths B and filling factors f of the magnetic elements, we calculated the LOS flux density $\Phi = B \times \cos \gamma \times f$, where γ denotes the angle between the LOS and the magnetic field, which is assumed to be perpendicular to the solar surface (lower right panel in Figure 3). The distribution of the LOS flux density Φ is also shown in Figure 3. Pixels with high LOS flux densities are not necessarily associated with high observed flux densities and inverted magnetic field strengths, mainly because of different filling factors.

The temperature can be derived for both the magnetic and non-magnetic components (see Figure 4). In both cases, the temperatures T_{mag} and T_{qS} correspond to an optical depth of $\log \tau_{500} = -1.5$. As long as the filling factor is not unity $f \neq 1$, the quiet Sun temperature T_{qS} is known for all pixels on the solar disk. The highest temperatures appear at disk center and the temperatures decrease towards the limb as expected for a typical limb darkening profile. The dependence of T_{qS} on μ can be well described by this fit

$$T_{\text{qS}}(\mu) = 3030.03 + 3729.23 \mu - 1835.61 \mu^2.$$

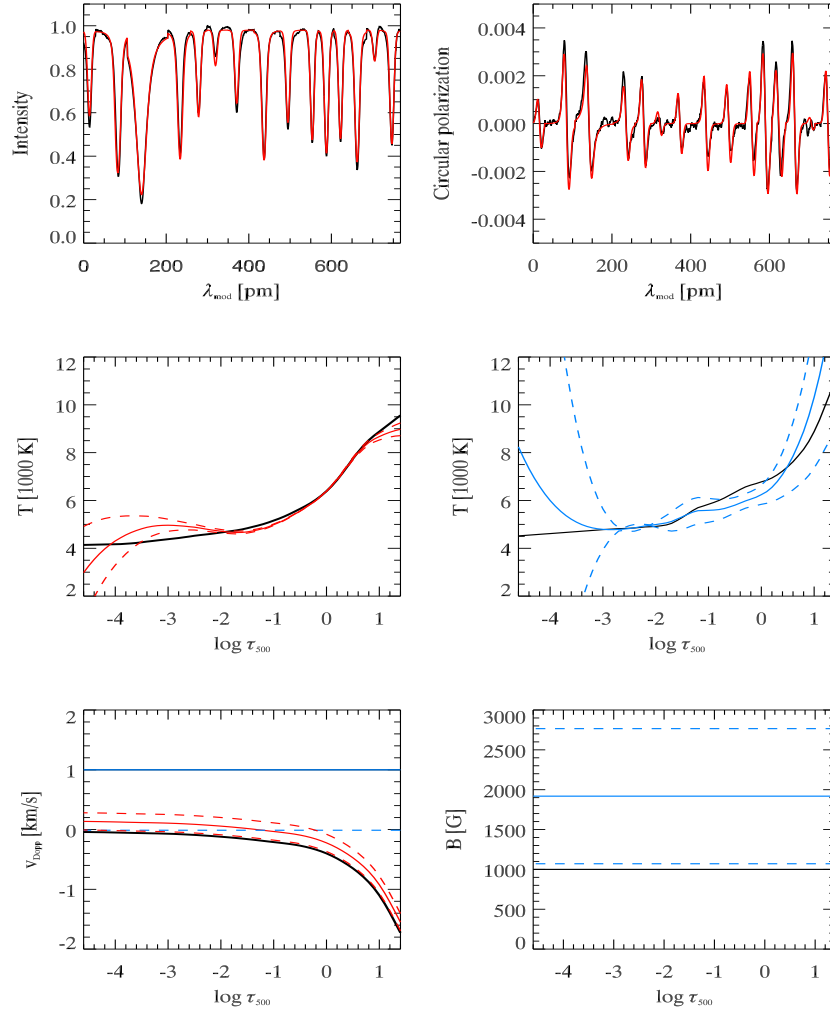


Figure 2. Comparison of observed (black) and inverted (red) Stokes I (upper-left) and Stokes V/I_c (upper-right) profiles. The inversion results are shown for one pixel close to disk center : temperatures T for the magnetic and non-magnetic (middle-left) and magnetic (middle-right) components, Doppler velocities v_{Dopp} (bottom-left), and magnetic field B (lower-right), Blue and red lines indicate the magnetic and non-magnetic components, respectively. The starting model is represented by solid black lines. Error limits of the inversion are given by the dashed lines. The wavelength scale is not continuous, *i.e.*, the spectral regions of interest are first extracted and then collated as in Demidov and Balthasar (2012).

The temperature of the magnetic component T_{mag} adds another diagnostic parameter for distinguishing between the two aforementioned populations. In the first population (see Figure 3), strong magnetic fields (1500–2000 G) are associated with high temperatures (5500–6500 K). In the second population, weak fields (50–150 G) are accompanied by low temperatures (5000–5300 K). The existence of two distinct populations also becomes clear, when the magnetic field strengths B are plotted against

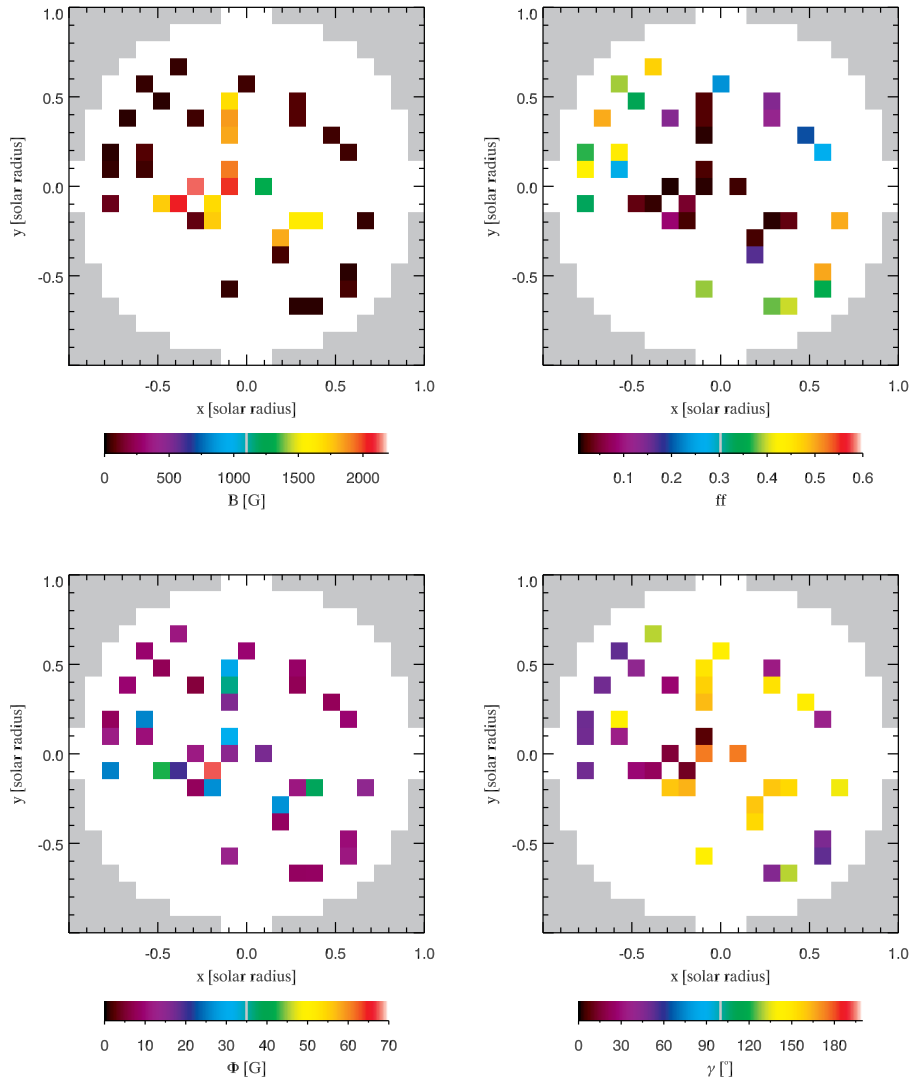


Figure 3. Inversion results for the magnetic field strength B (upper left), filling factor f (upper right), and the LOS magnetic flux density Φ (lower left). The angle γ in the selected pixels is displayed in the lower right panel.

the temperatures T (Figure 5). There, the transition from the weak to the strong regime does not occur smoothly but rather abruptly at a temperature of about 5300 K.

In previous investigations (Demidov and Balthasar, 2009, 2012), we showed that for some combinations of spectral lines, the magnetic flux density ratios R have a rather strong CLV. The pair of Fe I $\lambda 523.3$ nm and $\lambda 525.0$ nm lines had the strongest CLV. Therefore, we explored this combination of lines in more detail by computing the flux density ratios separately for both populations (Figure 6). Two well-separated regression

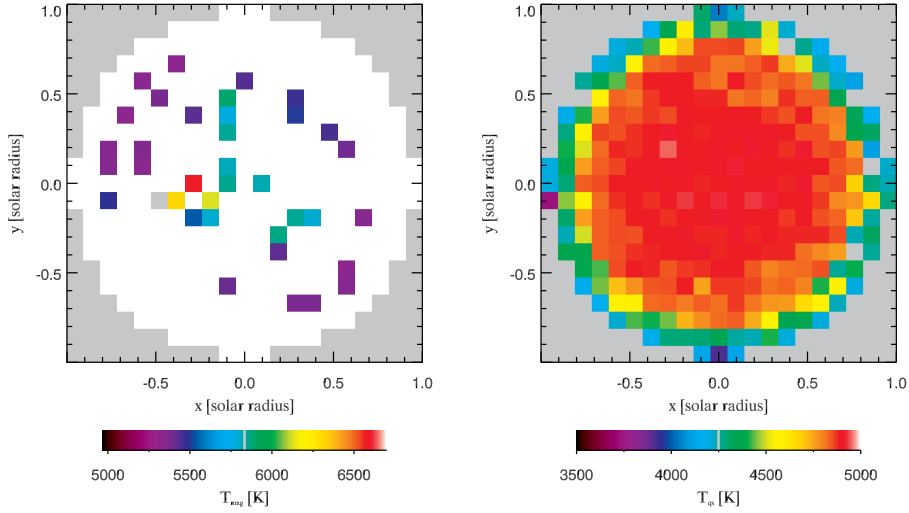


Figure 4. Inversion results for the temperature T of the magnetic (left) and non-magnetic (right) components at an optical depth of $\log \tau_{500} = -1.5$.

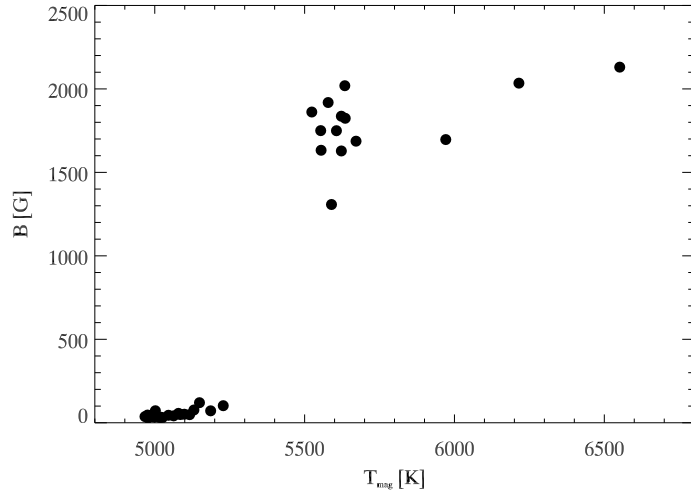


Figure 5. Comparison of the inverted magnetic field strengths B and temperature T , where B is constant with depth and T corresponds to an optical depth of $\log \tau_{500} = -1.5$.

lines are clearly visible yielding flux density ratios of $R_w = 1.71$ and $R_s = 2.35$ for the weak and strong populations, respectively. Even a few abnormal pixels near disk center, which have weak magnetic fields and large filling factors, would seamlessly fit onto the regression curve for the second population. This might be an indication that the two populations have a certain spatial overlap. Thus, the flux density ratios could be a better discriminator of the two populations rather than the heliocentric angle.

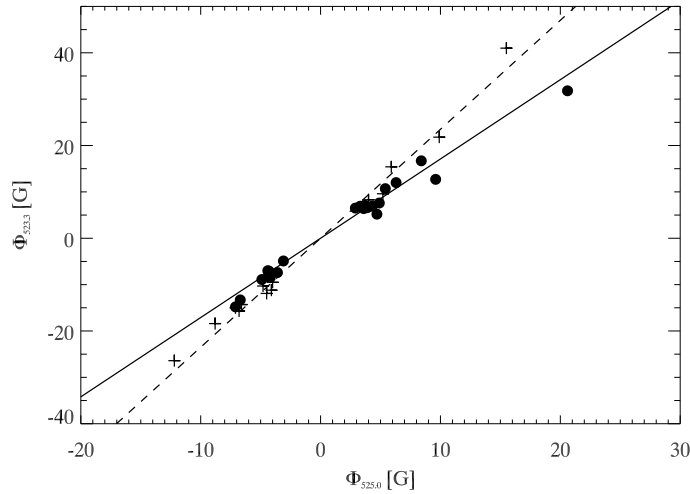


Figure 6. Scatter plots for the magnetic flux densities ϕ of the two Fe I $\lambda 523.3$ nm and $\lambda 525.0$ nm lines. Linear regression models are shown for both the weak (bullets) and strong (plusses) populations (see Figure 5).

4. Discussion and Conclusion

In this study, we have exploited the SIR code’s capability to simultaneously handle many spectral lines using two independent model components inside the resolution element so that it becomes possible to extract the height dependence of many physical parameters. On the other hand, the SIR code works only in the local thermodynamical equilibrium (LTE) approximation, with plane-parallel atmospheres, and depth-independent filling factors. This has to be considered in interpreting the results. Solar magnetic fields are supposed to exist as kilo-Gauss magnetic elements (magnetic flux tubes), which are distributed all over the solar surface. One place differs from another only by the concentration of these elements (filling factor) inside the resolution element (Stenflo, 1973). Therefore, we expected at the outset of our study that the SIR code would always provide kilo-Gauss magnetic fields for the magnetic component with different but small filling factors depending on the observed polarization signal. However, this assumption holds only for locations, which are close to disk center. In contrast, closer to the limb, weak magnetic fields with large filling factors and low temperatures are commonly encountered.

The dependence of the two populations with weak and strong magnetic fields on the heliographic angle points to the geometry of flux tubes as a possible explanation. Features with high magnetic field strengths are related to small filling factors. Thus, their horizontal extension must be small. Because of the high field strengths, the gas pressure in these flux tubes is low, and they are more transparent than their surroundings. They are heated through their walls and appear hot. If these features are close to vertical with respect to the solar surface, they are inclined to the LOS at a distance from disk center. An observer sees only the higher part of these features, and close to the limb, such features would be difficult to detect. In high photospheric layers, the magnetic flux

tubes must expand because of the lower outside pressure. In these layers, the magnetic field has a horizontal component, which might contribute to the circular polarization at locations away from the disk center, if the part towards the observer has more weight than that on the opposite side. There are two possible reasons for such a higher weight: (1) the optical path through the line-forming layers might not be sufficiently long to also reach the opposite side, or (2) the magnetic field lines are more (anti-)parallel to the LOS on the side towards the observer than on the opposite side. Consequently, features with low magnetic field strengths are more frequent closer to the limb, and they are related to lower temperatures. This geometric interpretation is in agreement with the findings of Bommier (2011) for internetwork magnetic fields. However, we cannot exclude based on our observations that the flux tubes with strong fields belong to the network.

Recently, Stenflo (2010, 2011) also discovered two populations of weak and strong magnetic fields in high-resolution *Hinode* Fe I $\lambda 630.15$ nm and $\lambda 630.25$ nm magnetograms. The detection of these strong and weak magnetic fields in two independent investigations with completely different data sets is certainly of general interest and warrants further scrutiny.

Acknowledgements We express our thanks to C. Denker for extended discussions and many suggestions which significantly improved this article, and P. Gömöry for carefully reading the manuscript. This work was supported by the Deutsche Forschungsgemeinschaft (BA 1875/6-1). MLD would like to express his appreciations to SOC/LOC of ESPM-13 for financial support which allowed him to attend the conference.

References

- Bommier, V.: 2011, *Astron. Astrophys.* **530**, A51.
- Borrero, J.M., Tomczyk, S., Kubo, M., Socas-Navarro, H., Schou, J., Couvidat, S., Bogart, R.: 2010, *Solar Phys.* **273**, 267.
- Danilovic, S., Schüssler, M., Solanki, S.K.: 2010, *Astron. Astrophys.* **513**, A1.
- Demidov, M.L., Zhigalov, V.V., Peshcherov, V.S., Grigoryev, V.M.: 2002, *Solar Phys.* **209**, 217.
- Demidov, M.L., Golubeva, E.M., Balthasar, H., Staude, J., Grigoryev, V.M.: 2008, *Solar Phys.* **250**, 279.
- Demidov, M.L., Balthasar, H.: 2009, *Solar Phys.* **260**, 261.
- Demidov, M.L., Balthasar, H.: 2012, *Solar Phys.* **276**, 43.
- Gingerich, O., Noyes, R.W., Kalkofen, W., Cuny, Y.: 1971, *Solar Phys.* **18**, 347.
- Ishikawa, R., Tsuneta, S.: 2011, *Astrophys. J.* **735**:74.
- Kontogiannis, I., Tsiropoula, G., Tziotziou, K.: 2011, *Astron. Astrophys.* **531**, A66.
- Manzo Sainz, R., Martínez González, M.J., Asensio Ramos, A.: 2011, *Astron. Astrophys.* **531**, L9.
- Norton, A.A., Pietarila Graham, J., Ulrich, R.K., Schou, J., Tomczyk, S., Liu, Y., Lites, B.W., López Ariste, A., Bush, R.I., Socas-Navarro, H., Scherrer, P.H.: 2006, *Solar Phys.* **239**, 69.
- Pierce, A.K., Slaughter, C.D.: 1977, *Solar Phys.* **51**, 25.
- Ruiz Cobo, R., del Toro Iniesta, J.C.: 1992, *Astrophys. J.* **398**, 375.
- Solanki, S.K., Briljjevič, V.: 1992, *Astron. Astrophys.* **262**, L29.
- Stenflo, J.O.: 1973, *Solar Phys.* **32**, 41.
- Stenflo, J.O.: 2010, *Astron. Astrophys.* **517**, A37.
- Stenflo, J.O.: 2011, *Astron. Astrophys.* **529**, A42.
- Suematsu, Y., Tsuneta, S., Ichimoto, K., Shimizu, T., Otsubo, M., Katsukawa, Y., Nakagiri, M., Naguchi, M., Tamura, T., Kato, Y., *et al.*: 2008, *Solar Phys.* **249**, 197.
- Thornton, L.M., Parnell, C.E.: 2011, *Solar Phys.* **269**, 13.